

The Chemical and Dynamical Evolution of Isolated Dwarf Galaxies

Kate Pilkington, Brad K. Gibson, Francesco Calura,
Greg S. Stinson, Chris B. Brook and Alyson Brooks

Abstract Using a suite of simulations [2] which successfully produce bulgeless (dwarf) disk galaxies, we provide an analysis of their associated cold interstellar media (ISM) and stellar chemical abundance patterns. A preliminary comparison with observations is undertaken, in order to assess whether the properties of the cold gas and chemistry of the stellar components are recovered successfully. To this end, we have extracted the radial and vertical gas density profiles, neutral hydrogen velocity dispersion, and the power spectrum of structure within the ISM. We complement this analysis of the cold gas with a brief examination of the simulations' metallicity distribution functions and the distribution of α -elements-to-iron.

1 Introduction

Historically, simulating the formation and evolution of a bulgeless, rotating, stellar disk, within the context of the classical picture of hierarchical assembly, has proven problematic [1]. Overcoming this has only been achieved recently [2], with Governato et al. presenting simulated dwarfs with bulge-to-disk ratios <0.04 , with very shallow associated central dark matter profiles. This was achieved by resolving the inhomogeneous ISM, thereby allowing for the imposition of a realistic star formation density threshold which resulted in strong supernovae-driven outflows preferentially removing low angular momentum gas.

In what follows, we concentrate our analysis on three simulated dwarf galaxies, the basic properties for two of which (DG1, DG1LT) have been introduced previously [2]. In §2, we quantify the spatio-kinetic characteristics of these bulgeless dwarfs, and contrast them with recent observational work [4, 5, 6]. A preliminary analysis of the chemical properties of the associated stellar components is then presented in §3 and compared with relevant empirical work in the field [7, 11]. As the

Kate Pilkington
Jeremiah Horrocks Inst, Univ of Central Lancashire, Preston, UK e-mail:
kpilkington@uclan.ac.uk

simulations are not modelled on any one particular galaxy, the analysis should be seen as comparative only in a qualitative sense.

1.1 Simulations

The three simulations analysed were run using the N-body+SPH code GASOLINE [10], employing the same initial conditions, and differing only in the adopted resolution, star formation density threshold, feedback efficiency, and star formation efficiency. The base simulation (DG1) [2] uses a star formation density threshold a thousand times higher (100 cm^{-3}) than that adopted in previous cosmological simulations ($\sim 0.1 \text{ cm}^{-3}$); a lower density threshold version (DG1LT), despite its possession of classical problematic traits (i.e., centrally-concentrated light ($B/D \approx 0.3$) and dark matter density distributions), is included here for comparison. This implementation of a more realistic density threshold for star formation was made possible by the associated high force resolution (86pc) which allowed us to resolve individual star forming regions of mass $\sim 10^5 M_{\odot}$. We include in our analysis a new simulation (nDG1), similar to DG1, but with two important modifications - the inclusion of high-temperature ($T > 10^4 \text{ K}$) metal-line cooling [9], and enhanced supernova feedback (100% of the energy being coupled to the surrounding ISM in the form of thermal energy, rather than the 40% used in the base simulation). The feedback method is described fully in [8].

2 HI Analysis of the Simulated Dwarfs

Throughout our analysis, we cross-check results which are based on cold gas particles ($T < 15000 \text{ K}$) [8] with those based on the inferred neutral hydrogen, to ensure our comparisons with empirical data have not been biased in any obvious manner. As the current implementation of ISM physics within GASOLINE does not allow gas to cool to densities more appropriate to molecular hydrogen, what we label as ‘HI’ can possess column densities $\sim 5\text{-}10\times$ larger than encountered in nature. For that reason, one must be careful to not overinterpret the quoted surface densities.

2.1 Radial Density Profiles

We first examine the radial density profiles of the cold gas in the three simulations (Fig 1). Observations of HI disks [6, 4] show that, in nature, they extend from ~ 2 to ~ 6 radial disk scalelengths and truncate near $\sim 1.5r_d$. DG1LT shows a flat profile with a formal scalelength of $\sim 18 \text{ kpc}$, which truncates at $\sim 0.5r_d$. The base simulation (DG1) has a radial scalelength of $\sim 6 \text{ kpc}$ (which is also approximately where it truncates); embedded within this extended disk is a high density cold gas core. Our new simulation (nDG1) can really only be fit using two exponentials, spanning the inner and outer disks (such double exponentials are fairly common in nature), and also possesses a compact cold core. These cores are somewhat transient, being

disrupted during periods of more significant star formation; e.g., for DG1, at $z \sim 0.7$ (the last epoch of substantial star formation - $0.1 M_{\odot}/\text{yr}$ compared to $0.005 M_{\odot}/\text{yr}$ at the present-day), the cold core is absent. These conclusions are robust to the choice of ‘HI’, as opposed to ‘cold gas’.

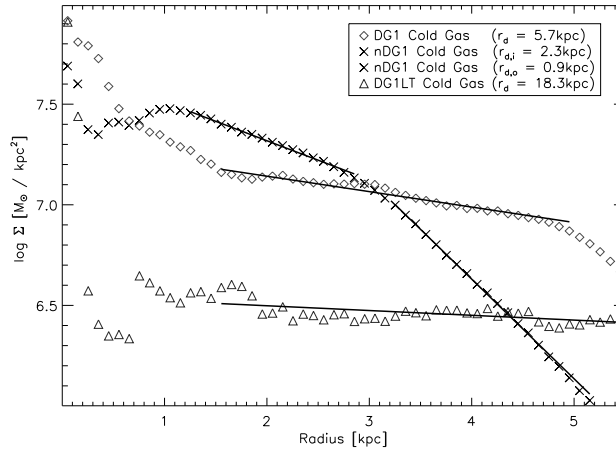


Fig. 1 Radial cold gas density profiles for the simulated dwarfs DG1 (diamonds), DG1LT (triangles), and nDG1 (crosses). The thick overplotted lines show the exponential fits to the distributions, from which the noted scalelengths were derived. nDG1 is best represented by a double exponential, with a break between the two near ~ 3 kpc. The cold gas of DG1 is distributed in a more extended exponential disk component of scalelength ~ 6 kpc, while that of DG1LT is ~ 18 kpc.

2.2 Flaring

Both DG1 and nDG1, when viewed edge-on, show significant flaring of their gas disks. In nature, comparable dwarfs [4] typically show an increase in the FWHM of their vertical density distribution of $\sim 50\%$ in going radially from $0.4r_d$ to $1.0r_d$. Fig 2 shows the vertical density profiles for the simulations at three annuli ($0.1r_d$, $0.4r_d$, and $1.0r_d$); we can see that DG1 flares by a factor of ~ 4 from $0.4r_d$ to $1.0r_d$, while nDG1 flares by a factor of ~ 1.5 . In that ‘fractional’ sense, DG1 seems somewhat extreme, but quantifying the flaring in terms of physical units (kpc), the degree of flaring is not dissimilar to that observed [4].

2.3 Velocity Dispersion

Observations of HI velocity dispersion profiles [6], for both giants and dwarfs, show that galaxies possess characteristic dispersions of $\sim 8\text{--}10\text{ km/s}$ (rising to $\sim 12\text{--}15\text{ km/s}$ in the inner star forming part of the disk). In Fig 3, we show the

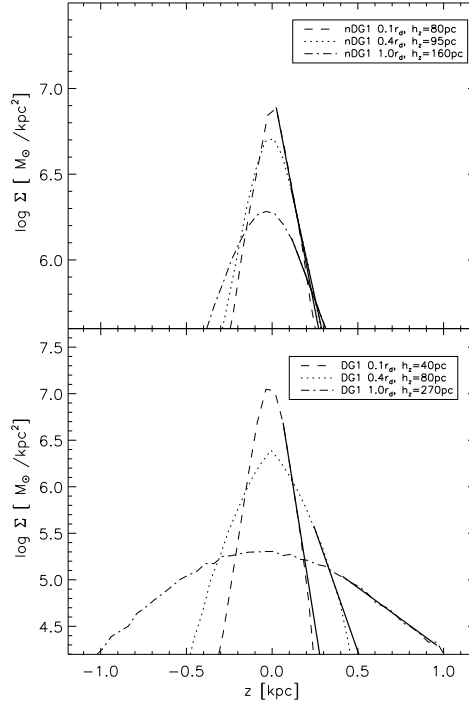


Fig. 2 Vertical density profiles of the cold gas disks for nDG1 (upper panel) and DG1 (lower panel), where ‘cold’ here means gas particles with temperatures less than 15000 K. The profiles are measured in three separate annuli corresponding to 0.1, 0.4, and 1.0 HI disk scale lengths. Overlaid on the plots are the exponential fits from which we derived the associated scaleheights (inset to each panel).

HI line-of-sight velocity dispersion profiles for nDG1, DG1LT, and Holmberg II [6]. Critically, we show nDG1 with (squares) *and* without (crosses) the inclusion of thermal broadening, following the methodology of [12]. Because SPH tracks only the streaming motions of the gas particles, one must incorporate the random velocity component to each particle, using the internal energy of each particle as input. In practice, we draw random velocities for each Cartesian coordinate from a Gaussian with $\sigma = \sqrt{kT/\mu}$ and add those to the components of the streaming motion. Without the inclusion of thermal broadening, nDG1 (and DG1) shows an extremely (and unphysically) kinematically cold ISM compared to that of DG1LT (which despite its aforementioned problems, resembles empirical data such as HoII very well). Two unresolved issues which are apparent from Fig 3 are that (i) while the dispersion based upon the streaming velocities (crosses) shows the same increase in the star forming portion of the disk that is observed in nature [6], the magnitude of the thermal broadening essentially “wipes out” this signal, and (ii) the velocity ellipsoid of the cold gas becomes isotropic, disguising any anisotropies that might have been present in the streaming motions (i.e., young stars, and the cold gas from which they formed, will necessarily have different velocity ellipsoids).

When DG1 is viewed at redshift $z \sim 0.7$, the more turbulent ISM being driven by the enhanced and sustained star formation ($0.1 M_{\odot}/\text{yr}$ compared to $0.005 M_{\odot}/\text{yr}$), was a close match to the velocity dispersion profiles observed in nature - put another

way, the dispersion of the streaming motions during periods of significant star formation are already on the order of the dispersions observed in nature, without the application of thermal broadening. As the gas clouds out of which stars are forming within these simulations have temperatures on the order of $\sim 8000\text{K}$, there is no way to avoid the imposition of a significant $\sim 8\text{ km/s}$ thermal broadening term; until we can resolve densities corresponding to cores of molecular clouds, this SPH limitation must be observed.

2.4 Power Spectrum

We next derived the spatial power spectra of the HI gas associated with our simulations, as well as that for the Small Magellanic Cloud [5], as shown in Fig 4, using Fourier Transforms of the moment zero density maps, after [5]. In the simulated galaxies, we smoothed with a 100pc Gaussian to be consistent with the beam smearing present in the observational data. All of the galaxies were then fit with a power law $P \propto k^\gamma$, where $\gamma = -3.5$ for DG1, $\gamma = -3.4$ for DG1LT, $\gamma = -4.2$ for nDG1, and $\gamma = -3.2$ for the SMC. The steeper slope possessed by nDG1 indicates an excess of power distributed on large scales within its simulated ISM, relative to that observed in the other simulations or the SMC (i.e., the enhanced feedback has shifted power from smaller scales to larger ones). The observational data (for the SMC and other dwarfs) is well fit by a pure power law, indicative of a lack of preference in HI cloud size, in nature), while the simulations show departures from this scenario. These departures can be traced to specific structures in the simulations - e.g., in nDG1, the enhanced power seen on scales of $\sim 400\text{--}500\text{pc}$ corresponds to the spacing of the tightly-wound spiral structures seen in its inner few kpcs.

3 Chemistry of the Simulated Dwarfs

The next direction for our work will be based upon a comparison of the stellar chemistry of the simulations with existing observational data. To date, we have examined the metallicity distribution functions (MDFs) and oxygen-to-iron distributions. Here, we simply highlight preliminary results pertaining to nDG1.

Fig 5 shows the present-day cumulative [Fe/H] MDF for all stars within 4 kpc of the three simulations, normalised to unity (arbitrarily) at [Fe/H] = -2.3 . Focusing on the metal-poor tail, it is apparent that our simulated dwarfs suffer from a ‘‘G-dwarf problem’’ (relative overproduction of metal-poor stars), an issue to which we will return in an upcoming study.

The global MDFs of the simulations are similar to those seen in Local Group dwarfs, with an ~ 0.16 dex dispersion ‘peak’ at [Fe/H] ≈ -1.1 superimposed on a broader metal-poor component (the formal dispersion of entire nDG1 MDF being ~ 0.32 dex). This is not dissimilar to the ~ 0.25 dex (intrinsic) dispersion seen (for example) in the Local Group dwarf, Carina [3]. While nDG1 is not a dwarf spheroidal, it does have an episodic star formation history akin to that of Carina.

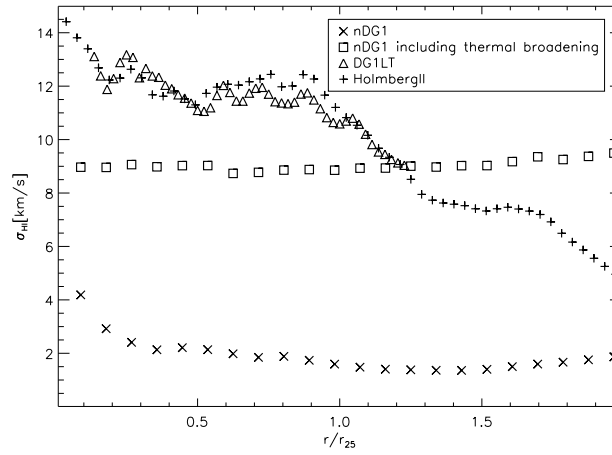


Fig. 3 HI line-of-sight (40° viewing angle) velocity dispersion profiles of nDG1 (crosses: particle streaming motions only), nDG1 with the inclusion of thermal broadening (squares), DG1LT (triangles), and observational data for Holmberg II (plus signs), scaled to r_{25} in the B-band (isophotal radius corresponding to 25 mag/arcsec^2 , roughly the extent of the star forming disk).

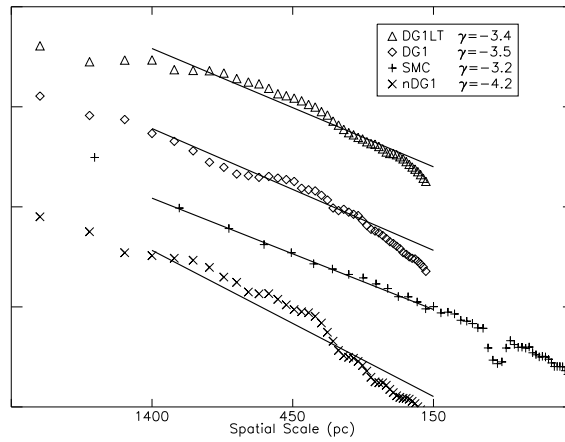


Fig. 4 Power spectra of the HI distributions of the three simulations - nDG1 (crosses), DG1 (diamonds), and DG1LT (triangles) - accompanied by that for the SMC. We truncated the power spectra for the simulations at $\sim 200 \text{ pc}$ (twice the beam size used to simulate the effects of beam smearing). The break in the SMC spectrum is due to a missing base line [5]. Overplotted on each dataset is a representative power law fit to the data, with the slopes noted in the inset to the panel.

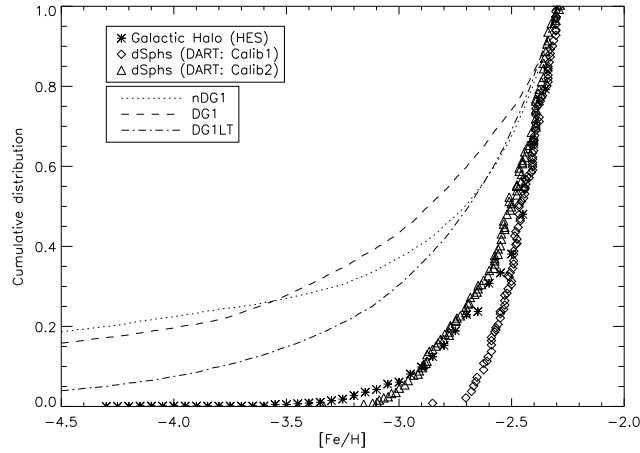


Fig. 5 Cumulative MDFs for nDG1 (dotted line), DG1 (dashed line) and DG1LT (dot dashed line). The compilation of observational data shown [7] includes that of the Galactic halo (asterisks) and the combined MDF constructed by merging those of the Carina, Sextans, and Sculptor dwarfs from DART data using two different metallicity calibrations (triangles and diamonds).

Fig 6 shows the relationship between $[O/Fe]$ and $[Fe/H]$ for the same stars (black dots) within 4 kpc of nDG1. Overplotted, again not because it is supposed to be a true analog of nDG1 but because it provides a useful benchmark, are the $[\alpha/Fe]$ - $[Fe/H]$ data (asterisks) for the Local Group dwarf, Sculptor [11]. The distribution of the residuals in $[O/Fe]$ about the best-fit lines through the Sculptor and nDG1 datasets are both consistent with intrinsic scatters of ~ 0.13 dex. For nDG1, this scatter varies somewhat with metallicity, with the scatter in the $[O/Fe]$ residuals for stars near $[Fe/H] \approx -1$ being ~ 0.1 dex, while those with $[Fe/H] < -1.5$ show a scatter closer to ~ 0.2 dex. To first order though, it would suggest that the adopted magnitude of metal diffusion employed was reasonable

References

1. Governato, F., Willman, B., Mayer, L., et al.: Forming disc galaxies Λ CDM simulations. *MMNRAS* **374**, 1479–1494 (2007)
2. Governato, F., Brook, C., Mayer, L., et al.: Bulgeless dwarf galaxies and dark matter cores from supernova-driven outflows. *Nature* **463**, 203–206 (2010)
3. Koch, A., Grebel, E.K., Wyse, R.F.G., et al.: Complexity on small scales: the metallicity distribution of the Carina dwarf spheroidal galaxy. *AJ* **131**, 895–911 (2006)
4. O’Brien, J.C., Freeman, K.C. and van der Kruit, P.C.: The dark matter halo shape of edge-on disk galaxies. III. Modelling the HI observations: results. *A&A* **515**, A62 (2010)
5. Stanimirovic, S., Staveley-Smith, L., Dickey, J.M., Sault, R.J. and Snowden, S.L.: The large-scale HI structure of the Small Magellanic Cloud. *MNRAS* **302**, 417–436 (1999)

6. Tamburro, D., Rix, H.-W., Leroy, A. K., et al.: What is driving the HI velocity dispersion? *ApJ* **137** 4424–4435 (2009)
7. Schörck, T., Christlieb, N., Cohen, J. G., et al.: The stellar content of the Hamburg/ESO survey. V. The metallicity distribution function of the Galactic halo. *A&A* **507**, 817–832 (2009)
8. Stinson, G., Seth, A., Katz, N., et al.: Star formation and feedback in smoothed particle hydrodynamic simulations - I. Isolated galaxies. *MNRAS* **373** 1074–1090 (2006)
9. Shen S., Wadsley, J., and Stinson, G.: The enrichment of the intergalactic medium with adiabatic feedback - I. Metal cooling and metal diffusion. *MNRAS* **407**, 1581–1596 (2010)
10. Wadsley, J.W., Stadel, J. and Quinn, T.: Gasoline: a flexible, parallel implementation of TreeSPH. *New Astronomy* **9** 137–158 (2004)
11. Tolstoy, E., Hill, V. and Tosi, M.: Star formation histories, abundances, and kinematics of dwarf galaxies in the Local Group. *ARAA* **47** 371–425 (2009)
12. van den Bosch, F.C., Abel, T. Croft, R.A.C., et al.: The angular momentum of gas in protogalaxies. I. Implications for the formation of disk galaxies. *ApJ* **576** 21–35 (2002)

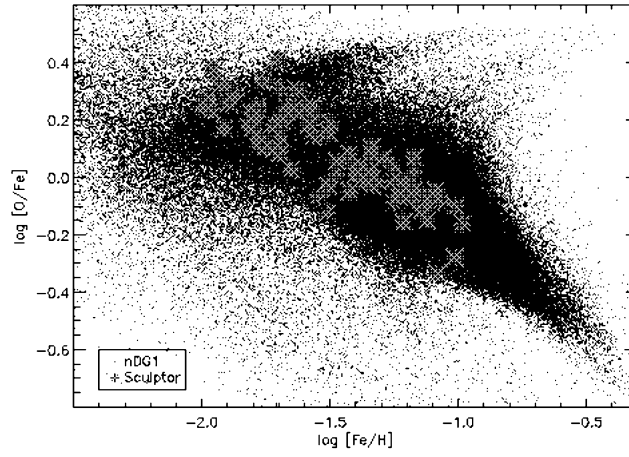


Fig. 6 $[\text{O}/\text{Fe}]$ - $[\text{Fe}/\text{H}]$ distribution for all stars within 4kpc of nDG1. For comparison, data from the Local Group dwarf, Sculptor[11], are overplotted (asterisks).